Engineering 25 (2023) 144–156

Contents lists available at ScienceDirect

Engineering

journal homepage: www.elsevier.com/locate/eng

Research
Frontiers of Chemical Engineering—Article

Engineering a Coordinatively Unsaturated Au–O–Ti^{3+} Structure Toward Unprecedented H_2 Efficiency for Low-Temperature Propene Epoxidation with H_2 and O_2

Zhaoning Song [a,#], Hao Yan [a,#], Juncong Yuan [a], Hongfei Ma [b], Jianlin Cao [a], Yongxiang Wang [c], Qiang Wang [c], Chong Peng [d,*], Feng Deng [c], Xiang Feng [a,*], De Chen [b], Chaohe Yang [a], Yongkang Hu [d]

[a] State Key Laboratory of Heavy Oil Processing, China University of Petroleum, Qingdao 266580, China
[b] Department of Chemical Engineering, Norwegian University of Science and Technology, Trondheim N-7491, Norway
[c] State Key Laboratory of Magnetic Resonance and Atomic and Molecular Physics, National Center for Magnetic Resonance in Wuhan, Innovation Academy for Precision Measurement Science and Technology, Chinese Academy of Sciences, Wuhan 430071, China
[d] State Key Laboratory of Fine Chemicals, School of Chemical Engineering, Dalian University of Technology, Dalian 116024, China

ARTICLE INFO

Article history:
Received 6 August 2022
Revised 2 December 2022
Accepted 11 January 2023
Available online 15 March 2023

Keywords:
Propene epoxidation
H_2 efficiency
Au/Ti bifunctional catalysts
Coordinatively unsaturated Ti
Density-functional theory

ABSTRACT

Since 1998, the Au–O–Ti^{4+} sites of Au/Ti-based catalysts have been widely accepted as the active sites for propene epoxidation with H_2 and O_2 at a relatively high temperature, although they are limited by poor H_2 efficiency. Herein, we demonstrate a novel Au–O–Ti^{3+} active site aiming at low-temperature propene epoxidation. Notably, this active site results in a sharp shift in the optimum temperature, from 200 to 138 °C, and allows the catalyst to maintain an unprecedented H_2 efficiency of 43.6%, a high propylene oxide (PO) selectivity of 90.7%, and a stability of over 100 h. The Au–O–coordinatively unsaturated Ti^{3+} active site is quantitatively constructed by tuning the amount of Si–OH and Bu_3NH^+ in post-treated silicalite-1 seeds. Through *operando* ultraviolet–visible (UV–vis) spectroscopy, the dynamic evolution of the Ti–OOH intermediate was investigated. It was found that the Ti–OOH generation rate is higher on Au–O–Ti^{3+} than on conventional Au–O–Ti^{4+} sites. Moreover, ammonia temperature-programmed desorption (NH_3-TPD) and X-ray photoelectron spectroscopy (XPS) characterizations, together with density-functional theory (DFT) calculations, demonstrated that the coordinatively unsaturated Ti^{3+} sites promote electron transfer between Au and Ti^{3+}, thereby enhancing the O_2 adsorption ability of the catalyst and promoting the *in situ* formation of H_2O_2 and the Ti–OOH intermediate, even at a low temperature. The insights and methodology reported here not only shed new light on maximizing H_2 efficiency over a coordinatively unsaturated Ti^{3+} structure of titanium silicate-1 but also open up new opportunities for industrial direct gas-phase propene epoxidation in a low temperature range.

1. Introduction

As an essential organic raw material, there is a tremendous market for propylene oxide (PO) in the chemical industry, where it is used for the manufacturing of polyether polyol, propylene glycol, and dimethyl carbonate. In this scenario, the utilization of propene, hydrogen (H_2), and oxygen (O_2) to manufacture PO provides a greener, simpler, and more sustainable route than traditional PO synthesis methods. In particular, this green process could liberate the industry from its reliance on traditional chlorohydrin and several organic hydroperoxide processes [1,2].

Since it was first reported in 1998 that gold (Au)/titanium dioxide (TiO_2) catalysts are efficient in direct propene epoxidation with H_2 and O_2 and possess the advantage of superior PO selectivity [3], many studies have focused on the development of Au/titanium (Ti)-containing support catalysts [4–11] to enhance their catalytic performance in industrial applications [12,13]. Au/titanium silicate-1 (TS-1), which possesses Au–O–Ti^{4+} active sites, has attracted a great deal of attention due to its remarkable

* Corresponding authors.
E-mail addresses: pengchong.fshy@sinopec.com (C. Peng), xiangfeng@upc.edu.cn (X. Feng).
# These authors contributed equally to this work.

https://doi.org/10.1016/j.eng.2023.01.008

high-temperature propene epoxidation performance with good C_3H_6 conversion (> 5.0%) and PO selectivity (> 90%). Unfortunately, Au/TS-1 catalysts still have the severe limitation of a low H_2 efficiency (only ~22.7%) [6,14–16]. Therefore, the precise construction of Au/Ti bifunctional catalysts and the identification of Au–Ti synergistic effects are highly desirable to overcome the above limitations.

It is notable that the *in situ* generation and decomposition of hydrogen peroxide (H_2O_2) can directly affect the H_2 efficiency of direct propene epoxidation with H_2 and O_2. A widely accepted reaction pathway has been provided, as follows: First, H_2O_2 is generated from H_2 and O_2 on Au nanoparticles [17,18]; subsequently, the H_2O_2 diffuses to nearby Ti active sites to generate Ti–OOH intermediates that epoxidize the propene to PO [19–21]. Thus, H_2 efficiency can be enhanced by promoting the synergy between Au nanoparticles and Ti sites. In recent years, in addition to the isolated tetrahedral Ti^{4+} species, other Ti species have been observed [22–27] and are assumed to be the active sites for activating H_2O_2. However, there are few studies on the synergistic effects of Au and coordinatively unsaturated Ti^{3+} sites on the *in situ* formation of H_2O_2. Along this route, there is an urgent need to precisely engineer novel Au/Ti bifunctional sites toward the development of industrially attractive Au/Ti bifunctional catalysts for the direct propene epoxidation reaction.

Herein, we devise a strategy to quantitively construct coordinatively unsaturated Ti^{3+} sites on a novel TS-1 (TS-1-cS) support by tuning the amount of Si–OH and Bu_3NH^+ in post-treated silicalite-1 (S-1) seed. Based on *operando* ultraviolet–visible (UV–vis) spectroscopy, *in situ* Fourier-transform infrared (FT-IR) spectroscopy, X-ray photoelectron spectroscopy (XPS), and density-functional theory (DFT) calculation, it is confirmed that the presence of coordinatively unsaturated Ti^{3+} sites promotes electron transfer between Au and Ti, thereby facilitating the formation of Au–O–Ti^{3+} active sites. Compared with traditional Au–O–Ti^{4+} sites, these Au–O–Ti^{3+} active sites are more conducive to O_2 adsorption and thus effectively promote the *in situ* generation of H_2O_2 and the formation of the active intermediate Ti–OOH. As a result, the Au/TS-1-cS catalyst has an excellent H_2 efficiency (43.6%) at a relatively low reaction temperature. We further provide a plausible structure–performance relationship between coordinatively unsaturated Ti^{3+} sites and H_2 efficiency. The insights and methodology reported here open up new opportunities for optimizing H_2 efficiency over the coordinatively unsaturated Ti^{3+} structure of TS-1 for novel low-temperature propene epoxidation.

2. Material and methods

2.1. Preparation of the catalysts

The synthesis of S-1 seed was performed following the process reported by Cundy et al. [28]. Subsequently, the S-1 seeds were processed and etched using *n*-butylamine at different concentrations (0.6, 1.2, and 1.8 mol·L^{-1}), as follows: A certain amount of *n*-butylamine (99.5 wt%; Sinopharm Chemical Reagent Co., Ltd., China) and 2 g of S-1 seeds were dissolved in 30 mL of deionized water under stirring at room temperature for 0.5 h. The resulting mixture was transfused into a Teflon-lined stainless steel autoclave and hydrothermally crystallized at 443 K for 24 h. Finally, the crystalline solid was centrifuged and washed four times, and then dried at 303 K for 24 h. The as-prepared S-1 seed etched by *x* mol·L^{-1} *n*-butylamine is denoted as S-1-*x*M; for example, S-1-0.6M represents S-1 seed etched by 0.6 mol·L^{-1}*n*-butylamine.

The TS-1-cS support was prepared as follows: 5 g of *n*-butylamine (99.5 wt%) and 3 g of tetrapropylammonium hydroxide (TPAOH, 25 wt%; Sigma-Aldrich Chemical Inc., USA) were mixed in deionized water under stirring. Subsequently, 10 g of colloidal silica (Sinopharm Chemical Reagent Co., Ltd.) was added to this mixture. In the meantime, 0.4 g of titanium(IV) tetrabutoxide (TBOT, 99 wt%; Sinopharm Chemical Reagent Co., Ltd.) was dissolved in 20 mL of isopropanol (IPA, 99.5 wt%; Sinopharm Chemical Reagent Co., Ltd.). The Ti-containing mixture was added dropwise to the Si-containing mixture, while stirring. Afterward, 1 g of the aforementioned treated S-1 seed was poured into the mixture described above. The final solution was poured into a Teflon-lined stainless steel autoclave and hydrothermally crystallized at 443 K for 72 h. Finally, the crystalline solid was centrifuged and washed four times, dried at 393 K for 12 h, and then calcined at 823 K for 6 h. The as-prepared TS-1-cS support prepared with S-1-*x*M seed is denoted as TS-1-cS-*x*M. For example, TS-1-cS-0.6M represents TS-1-cS support prepared using S-1-0.6M seed. A conventional TS-1 with a similar Si/Ti ratio was synthesized using the hydrothermal method developed by Khomane et al. [29].

The deposition–precipitation method was employed to prepare a series of Au/TS-1-cS catalysts with a unified Au loading of 0.10 wt% [30]. In brief, 0.2 g of hydrogen tetrachloroaurate(IV) trihydrate ($HAuCl_4·4H_2O$, 99.99%; Sigma-Aldrich Chemical Inc.) was dissolved in 50 mL of deionized water. Subsequently, 0.5 g of TS-1-cS powder was dissolved in the solution with stirring. Subsequently, the solution was maintained at a pH of 6.5–7.5 by adding 1.0 and 0.1 mol·L^{-1} NaOH (Sinopharm Chemical Reagent Co., Ltd.) solution with stirring at 298 K for 9 h. The final seriflux was centrifuged and washed by centrifugation (5000 r·min^{-1} for 5 min) with ice deionized water, and then dried at 298 K for 12 h under vacuum.

2.2. Characterizations

^{29}Si magic-angle spinning (MAS) nuclear magnetic resonance (NMR) measurements were collected on a Varian Unity INOVA (600 MHz) spectrometer (Varian, USA). UV–vis spectra were recorded on a PerkinElmer LAMBDA 35 spectrophotometer (PerkinElmer, USA) over a wavelength range of 200–800 nm with pure $BaSO_4$ plate as the reference. The peak area at 220 nm was obtained through fitting and integrating according to the symmetry of the peak. Ammonia temperature-programmed desorption (NH_3-TPD) spectra were obtained on a Quantachrome ChemBET TPR/TPD (Quantachrome, USA). X-ray diffraction (XRD) patterns were collected on an X'pert PRO MPD diffractometer instrument (Panalytical, the Netherlands) using Cu Kα radiation. ^{31}P MAS NMR experiments were performed on a 9.4 T Bruker AVANCE III spectrometer (Bruker, Switzerland) using 4 mm rotors at a spinning frequency of 10 kHz (operating at a Larmor frequency of 161.7 MHz for ^{31}P). A pulse width of 3.0 μs corresponding to a $\pi/2$ flip angle, a recycle delay of 30 s, and a total of 1024 scans were used to collect single-pulse ^{31}P MAS NMR spectra. High-resolution transmission electron microscopy (HRTEM) images were taken on a JEOL JEM-2100F microscope (JEOL, Japan). *Operando* UV–vis spectra were collected on an AvaSpec-2048 spectrometer (Avantes, the Netherlands) equipped with a transmission dip probe. *In situ* FT-IR spectra were recorded on a Nicolet iS20 instrument (Thermo, USA) equipped with an HgCdTe (MCT) detector cooled by liquid nitrogen. XPS spectra were obtained using a PerkinElmer PHI 5000C ESCA system (PHI, USA), and the carbonaceous C 1s line (284.6 eV) was used as a reference to calibrate the binding energies.

2.3. Catalytic testing

The direct propene epoxidation reaction was reacted in a quartz tubular reactor with an inner diameter of 8 mm, containing 0.15 g of Au/TS-1-cS catalyst and utilizing a feed containing propene (C_3H_6), H_2, O_2, and nitrogen (N_2) with a flow rate of 3.5, 3.5, 3.5, and 24.5 mL·min^{-1}, respectively. The space velocity was 14 000 mL·h^{-1} per gram of catalyst. These conditions are consistent with the literature [1–4,14,15,19,25,29]. Subsequently, the series of Au/TS-1-cS catalysts were tested under atmospheric pressure at the relatively low temperature of 138 °C. The products were analyzed by means of an online gas chromatograph (Agilent 6890, Agilent, USA). A flame ionization detector (FID) with a Porapak T column was used to analyze the PO, ethanal, propanal, acetone, acrolein, and other oxygenates, while a thermal conductivity detector (TCD) was used to analyze the hydrocarbons, H_2, O_2, N_2, carbon dioxide (CO_2), and water (H_2O). Blank evaluations showed that no PO was produced in the catalyst-free reactor. The catalytic performances were calculated using a normalization method defined as follows:

$$C_3H_6\ \text{conversion} = \frac{n_{C_3\text{-oxy}} + \frac{2}{3}n_{\text{ethanal}} + \frac{1}{3}n_{CO_2}}{n_{C_3H_6,\text{in}}} \times 100\% \quad (1)$$

$$\text{PO selectivity} = \frac{n_{PO}}{n_{C_3\text{-oxy}} + \frac{2}{3}n_{\text{ethanal}} + \frac{1}{3}n_{CO_2}} \times 100\% \quad (2)$$

$$H_2\ \text{efficiency} = \frac{n_{PO}}{n_{H_2,\text{conv}}} \times 100\% \quad (3)$$

where $n_{C_3\text{-oxy}}$, n_{ethanal}, n_{CO_2}, $n_{C_3H_6,\text{in}}$, n_{PO}, and $n_{H_2,\text{conv}}$ are the moles of C_3-oxygenates, ethanal, CO_2, C_3H_6 in the feed, PO, and the converted H_2.

2.4. Density-functional theory calculations

All calculations were performed using the DMol^3 module of Materials Studio 8.0. The meta generalized gradient approximation (meta-GGA) in the form of M06-L was selected to describe the correlation and exchange effects, and double numerical plus polarization (DNP) was used to consider the electronic polarization effect. Brillouin-zone integrations with a smearing of 0.005*Ha* were used to improve the precise electronic convergence in the calculation. All the energies were corrected by means of the zero-point vibrational energy (ZPE). The allowable deviations of the displacement, gradient, and total energy were 0.0005 nm, 4.35×10^{-17} J·nm^{-1}, and 4.35×10^{-23} J, respectively. In the calculation process, a 46T TS-1 model (where T refers to Si or Ti) was used to represent the titanium silicon zeolite with an MFI structure. For the TS-1-Ti^{4+} model, T12 was replaced by a Ti atom to form the perfect tetracoordinated Ti species (Ti^{4+}) structure. For the TS-1-Ti^{3+} model, when T12 was replaced by a Ti atom, two –OH groups were added to form a type of coordinatively unsaturated hexacoordinated Ti^{3+} structure. Then, the Au_4 cluster was supported on the TS-1-Ti^{4+} and TS-1-Ti^{3+} to form the Au_4/TS-1-Ti^{4+} and Au_4/TS-1-Ti^{3+} models. The binding energy (BE) or adsorption energy was calculated using the following formula:

$$E_a = E_{\text{sub+mod}} - E_{\text{sub}} - E_{\text{mod}} \quad (4)$$

where E_{mod}, E_{sub}, $E_{\text{sub+mod}}$, and E_a are the energy of the bare model, the energy of the adsorbed or bound substrate, the total energy of the substrate on the calculation model, and the adsorption energy of adsorbate, respectively.

3. Results and discussion

3.1. A novel strategy to quantitively construct coordinatively unsaturated Ti^{3+} sites

A series of TS-1 supports with controllable coordinatively unsaturated Ti^{3+} sites (TS-1-cS) were developed to anchor Au precursors as bifunctional catalysts. First, TS-1-cS supports with controllable Ti^{3+} contents were prepared by regulating the properties of S-1 seeds. The ^{29}Si MAS NMR spectra of S-1 seeds treated by *n*-butylamine with different concentrations (i.e., 0.6, 1.2, and 1.8 mol·L^{-1}) are shown in Fig. 1(a). The Q3 peak at −102 ppm is ascribed to the $(SiO)_3SiOH$ groups, the higher Q4 peak at −111 ppm is ascribed to the $Si(OSi)_4$ groups, and the peak at −114 ppm is ascribed to the monoclinic structure. The relative Q3/Q4 ratio represents the relative content of $(SiO)_3SiOH$ in the S-1 seeds. As can be seen from Fig. 1(b), the relative Q3/Q4 ratio of the S-1 treated by 0.6 mol·L^{-1} *n*-butylamine is 0.205. With an increase in *n*-butylamine concentration, the relative Q3/Q4 ratio shows an upward trend, demonstrating a regular increase in the Si–OH proportion in the S-1 seeds, and the relative Q3/Q4 ratio of the S-1 treated by 1.8 mol·L^{-1} *n*-butylamine reaches 0.410. Thus, treating the S-1 seeds with *n*-butylamine with different concentrations resulted in different Si–OH proportions.

The amount of *n*-butylamine interacting with the S-1 seeds was characterized by means of inorganic elements analysis to test the corresponding nitrogen (N) element contents. The results showed that the N element contents of S-1-0.6M, S-1-1.2M, and S-1-1.8M were 0.89%, 1.17%, and 1.35%, respectively, indicating that the interaction between *n*-butylamine and S-1 seeds was strengthened as the concentration of *n*-butylamine increased. The pore structures of the S-1 seeds treated by *n*-butylamine with different concentrations were also investigated via N_2 physisorption characterization. The results are provided in Table S1 in Appendix A, which shows that the surface area and pore volume of S-1-*x*M seeds increase with an increase in *n*-butylamine treatment concentration. This difference in seed pore structure can lead to a change in the content of Si–OH defect sites, which is consistent with the results obtained via ^{29}Si MAS NMR. Fig. S1 in Appendix A shows transmission electron microscopy (TEM) images of the three S-1 seeds. The average crystal size of the three S-1 seeds is quite similar, at about 140 nm. The as-formed S-1 seeds were used to synthesize TS-1-cS.

The specific environment of the Ti species and the acidity of the TS-1-cS samples were studied in detail using inductively coupled plasma (ICP), UV–vis, ^{31}P MAS NMR, and NH_3-TPD characterizations. The Ti contents of TS-1-cS-0.6M, TS-1-cS-1.2M, and TS-1-cS-1.8M were found to be 2.07%, 2.10%, and 2.08%, respectively, indicating that the three supports had almost the same Ti content. Fig. 1(c) shows the detailed composition of the Ti species in the TS-1-cS samples. The peak at 220 nm can be attributed to the isolated tetracoordinated Ti species (Ti^{4+}), whereas the peak at 258 nm can be attributed to the pentacoordinated or hexacoordinated Ti species (Ti^{3+}) [22,25]. Therefore, the normalized area ratio ($A_{258nm}/A_{220nm+258nm}$, equal to $A_{Ti^{3+}}/A_{Ti^{4+}+Ti^{3+}}$) can be used as a descriptor to reflect the Ti^{3+} species proportion. As can be seen from Fig. 1(d), with an increase in Si–OH content in the S-1 seeds, the $A_{Ti^{3+}}/A_{Ti^{4+}+Ti^{3+}}$ ratio in the corresponding TS-1-cS samples gradually increases from 0.133 to 0.228, indicating that the relative content of the Ti^{3+} species regularly increases from TS-1-cS-0.6M to TS-1-cS-1.8M. This result is consistent with the result from XPS in Section 3.3; that is, the Ti^{3+} species content shows a regular increasing trend from TS-1-cS-0.6M to TS-1-cS-1.8M.

In addition, various titanium species can be distinguished by the different phosphorus signals of trimethyl-phosphine (TMP) on the zeolite. Fig. 1(e) shows the ^{31}P MAS NMR spectra of the TMP adsorbed on the series of TS-1-cS samples. The resonance peak at −4.5 ppm is assigned to the TMP adsorbed onto the sites (e.g. Si–OH–Ti, Ti–OH, or Si–OH) due to the Brønsted acidic properties of the TS-1-cS samples [31–33]. The resonance peak at −33.3 ppm is assigned to the TMP bound to the coordinatively unsaturated Ti sites [34,35], while the resonance peak at

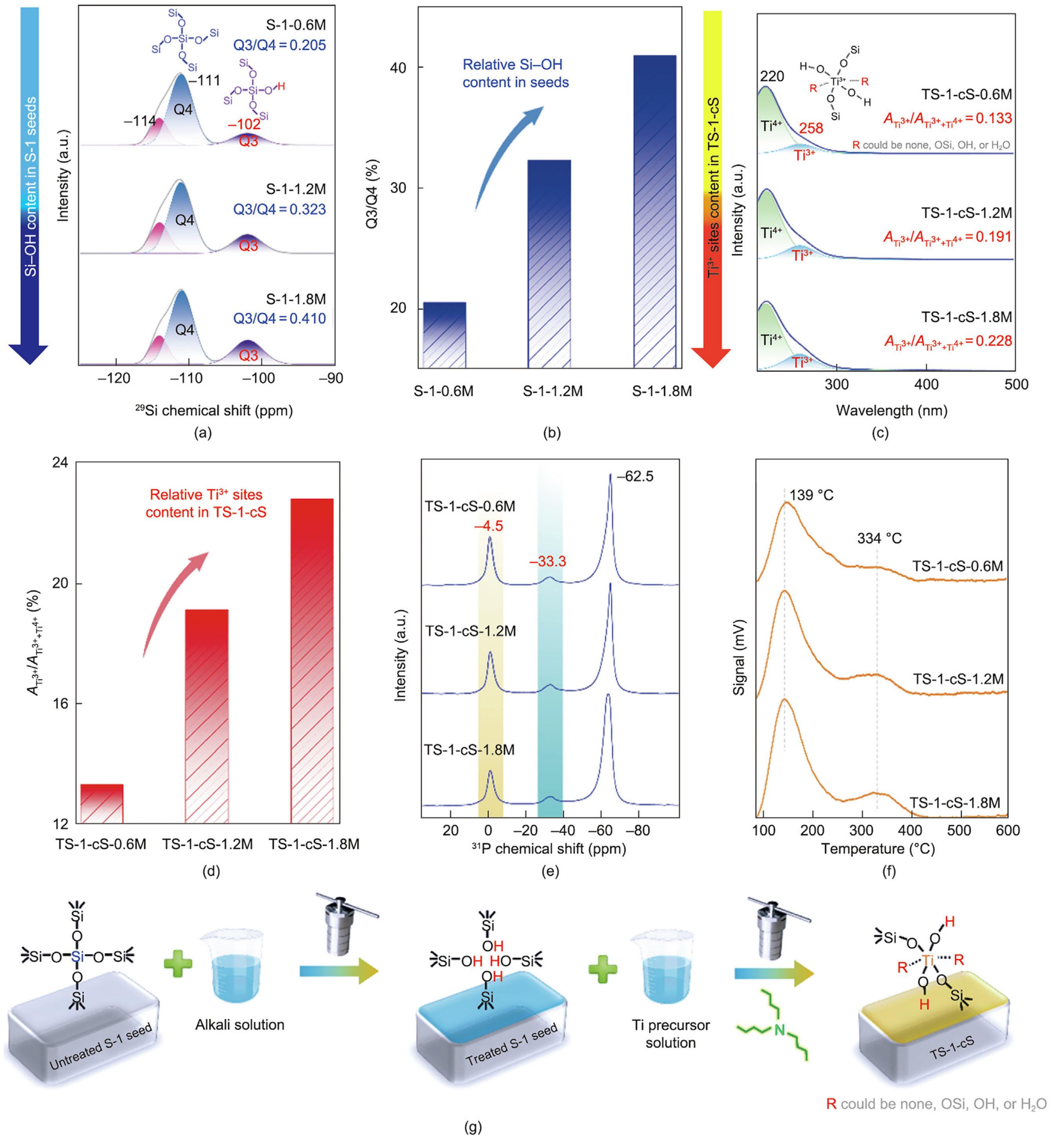

Fig. 1. (a) ^{29}Si MAS NMR spectra of S-1 seeds treated by different concentrations of *n*-butylamine. (b) Relative Q3/Q4 ratio of ^{29}Si MAS NMR spectra for the S-1 seeds. (c) UV–vis spectra and (d) relative $A_{Ti^{3+}}/A_{Ti^{4+}+Ti^{3+}}$ ratio of UV–vis spectra of the TS-1-cS supports. (e) ^{31}P MAS NMR and (f) NH_3-TPD spectra of corresponding TS-1-cS supports. (g) Plausible schematics of the TS-1-cS synthesis mechanism.

−62.5 ppm is ascribed to the physisorbed TMP [36]. It was found that the relative amount of coordinatively unsaturated Ti sites ($A_{-33.3ppm}/A_{(-33.3ppm)+(-4.5ppm)}$) shows a regular upward trend from TS-1-cS-0.6M to TS-1-cS-1.8M. Combined with the UV–vis characterization results described above, it can be found that the change trend in the Ti^{3+} species matches that of the coordinatively unsaturated Ti sites, which means that the coordinatively unsaturated sites are mainly composed of Ti^{3+} species.

NH_3-TPD was adopted to determine the total acidity of the TS-1-cS samples, as shown in Fig. 1(f). All the TS-1-cS samples exhibited two NH_3 desorption peaks at 139 and 334 °C, which are ascribed to weak and medium acid centers [37,38]. Although the desorption temperatures of the three samples are the same, the peaks of the TS-1-cS samples differ greatly in intensity. In addition, the amount of weak and medium acid sites gradually increases from TS-1-cS-0.6M to TS-1-cS-1.8M.

The synthesis mechanism of TS-1-cS was further analyzed, as shown in Fig. 1(g). It has been reported that, during the hydrothermal synthesis process, isomorphous substitution occurs between Si atoms in the seed framework and Ti atoms in the precursor solution [39–41]. Therefore, it can be assumed that the higher the content of Si–OH vacancies in the seed framework, the higher the content of coordinatively unsaturated Ti vacancies in the TS-1-cS that can be obtained via isomorphous substitution. Moreover, the surfaces of the S-1 seeds are grafted with Bu_3NH^+ after treatment with *n*-butylamine [42] in a strong alkali environment. Therefore, due to the insufficient amount of TPAOH, the Bu_3NH^+ in the seeds can play an auxiliary guiding role of a template agent in the synthesis process of TS-1-cS [43]. Furthermore, the Ti-containing tetrahedron structure is unstable because of the large ionic radius of Ti [44]. Therefore, coordinatively unsaturated Ti^{3+} species are likely to form with a weak template effect of Bu_3NH^+ [45]. In summary, the presence of Si–OH and Bu_3NH^+ in the S-1 seeds can induce the formation of coordinatively unsaturated Ti^{3+} species.

3.2. Low-temperature propene epoxidation performance at Au–O–Ti^{3+} sites

The series of Au/TS-1-cS catalysts were evaluated in low-temperature direct propene epoxidation with H_2 and O_2 (Fig. 2) at only 138 °C, which is much lower than the traditional temperature of 200 °C. As the Au/TS-1-cS catalyst with the least amount of coordinatively unsaturated Ti^{3+} species, Au/TS-1-cS-0.6M exhibited a stable PO formation rate of only 75.4 $g\cdot h^{-1}$ per kilogram of catalyst (kg_{cat}) and a H_2 efficiency of 29.8%. Obviously, with an increase in the content of coordinatively unsaturated Ti^{3+} species, the PO formation rate and H_2 efficiency of these Au/TS-1-cS catalysts gradually increased. As the content of the coordinatively unsaturated Ti^{3+} species in the TS-1-cS reached 22.8%, the PO formation rate and H_2 efficiency of Au/TS-1-cS-1.8M significantly rose to 135.7 $g\cdot h^{-1}\cdot kg_{cat}^{-1}$ and 43.6%, respectively. It is worth mentioning that the stable and high PO formation rate of Au/TS-1-cS-1.8M at the relatively low reaction temperature of 138 °C is comparable with that of a conventional Au/TS-1 catalyst with isolated Ti^{4+} species at the higher reaction temperature of 200 °C (155.1 $g\cdot h^{-1}$ per kilogram of TS-1; Fig. S2 in Appendix A). Moreover, a H_2 efficiency of 43.6% is unprecedented in low-temperature direct propene epoxidation with H_2 and O_2. However, with a further increase in the content of the coordinatively unsaturated Ti^{3+} species, the PO formation rate and H_2 efficiency of Au/TS-1-cS-2.4M showed a volcano trend, probably because an excessive number of Ti^{3+} sites can aggravate side reactions—that is, the ring-opening of PO. In addition, according to the thermogravimetric analysis (TGA) and derivative thermogravimetric (DTG) curves of the Au/TS-1-cS catalyst after the reaction at 138 °C for 40 h (Fig. S3 in Appendix A), the excellent stability of the Au/TS-1-cS catalysts is likely to be a result of the inhibition of coke formation due to the unique structure of TS-1-cS, which enhances the mass transfer capacity, as reported in our previous work [15,46,47].

Moreover, Fig. 2(d) shows that all the catalysts have a comparable PO selectivity of about 91%, indicating that the coordinatively unsaturated Ti^{3+} sites are not very sensitive to the occurrence of side reactions in low-temperature propene epoxidation. As shown in Fig. S4 in Appendix A, as the reaction temperature rises from 138 to 168 °C, the PO selectivity and H_2 efficiency rapidly plummet, while the PO formation rate rises constantly, indicating that the *in situ* generation rate of H_2O_2 continues to increase. However, a high proportion of H_2O_2 decomposes into H_2O, resulting in the plummeting in H_2 efficiency. The resulting large amounts of H_2O can cause a ring-opening side reaction of PO. As the reaction temperature continues to rise to 200 °C, the PO formation rate, PO selectivity, and H_2 efficiency all rapidly plummet further; the reaction quickly deactivates, and the side reaction is dominant.

At different reaction temperatures, the differences in the PO decomposition ability of the Au/TS-1-cS catalysts with different contents of coordinatively unsaturated Ti^{3+} were analyzed via *in situ* FT-IR characterization, with the results shown in Fig. 3. The bands at 2976.4, 2938.6, and 2886.7 cm^{-1} are assigned to the C–H stretching vibrations of the bidentate propoxy species, which can result from PO decomposition at acidic Ti sites [17,48]. The bands at 1720 cm^{-1} are assigned to the C=O stretching vibrations of oxides containing a C=O group (i.e., acetone, aldehyde, or propanal), which can also result from PO decomposition [48]. However, no significant differences are observed between the three catalysts at 1720 cm^{-1} (Fig. S5 in Appendix A), because the main byproducts produced from PO decomposition at the acidic Ti sites are bidentate propoxy species, rather than oxides.

As the reaction temperature increased from 140 to 200 °C, the content of the bidentate propoxy species in all samples increased, indicating that PO decomposition intensified with an increase in the reaction temperature. In addition, it is worth noting that the content of coordinatively unsaturated Ti^{3+} sites in the catalysts had little effect on PO decomposition at a lower reaction temperature (e.g., 140 °C). This finding suggests that a low temperature can significantly inhibit the decomposition of H_2O_2 and dramatically suppress the cleavage of C–O and C–C bonds at the Ti^{3+} acidic sites [25,38,49,50].

It is notable that H_2 efficiency is an important factor affecting catalytic performance in this reaction [25,51,52]. Due to the boosted H_2 efficiency, the Au/TS-1-cS catalyst is more effective at forming Ti–OOH and subsequent PO. The higher H_2 efficiency is likely to be affected by both the Au sites and the coordinatively unsaturated Ti^{3+} species [53–55]. Therefore, it was preliminarily speculated that the coordinatively unsaturated Ti^{3+} species may promote metal–support interaction, thereby promoting the formation of H_2O_2. This speculation will be discussed in detail later in Section 3.3.

3.3. Intrinsic reasons for the unique H_2 efficiency promoted by the coordinatively unsaturated Ti^{3+} sites

H_2 efficiency is a key aspect in the direct propene epoxidation reaction system with H_2 and O_2. According to recent studies [25,56–58], the H_2 efficiency for this reaction system is defined as the ratio of moles of PO generated to those of H_2 converted. For the Au–O–Ti bifunctional active sites, both the Au and Ti species can influence the catalytic performance. The *in situ* generation of H_2O_2 from H_2 and O_2 on Au nanoparticles is the key step in this reaction. Therefore, the physicochemical properties of the Au in the catalysts were studied first, in order to elucidate the intrinsic reason for the significant changes we observed in catalyst activity and H_2 efficiency (Fig. 4). The ICP results showed that the Au loading of the Au/TS-1-cS-0.6M, Au/TS-1-cS-1.2M, and Au/TS-1-cS-1.8M catalysts was about 0.1 wt%, indicating that the three catalysts have similar Au loadings. Considering that the size effect of Au nanoparticles is a key element in the reaction [4,7,16,59,60], HRTEM was used to study the size distribution and lattice spacing of the Au nanoparticles in the Au/TS-1-cS catalysts. Figs. 4(a)–(c) show that all catalysts exhibit similar average sizes (3.0 nm) of Au nanoparticles, which can eliminate the influence of the Au size effect on catalytic performance [2,61–65]. In addition, Figs. 4(d)–(f) show that the lattice spacing of the Au nanoparticles in the three catalysts is 0.23 nm, corresponding to Au(111), which is a stable surface for Au nanoparticles.

The other key factors affecting the reaction are the structure and crystal morphology of the support. Figs. 4(g)–(i) show that all samples are in the shape of a cuboid with similar average crystal sizes of about 150 nm × 120 nm × 105 nm, which is due to the

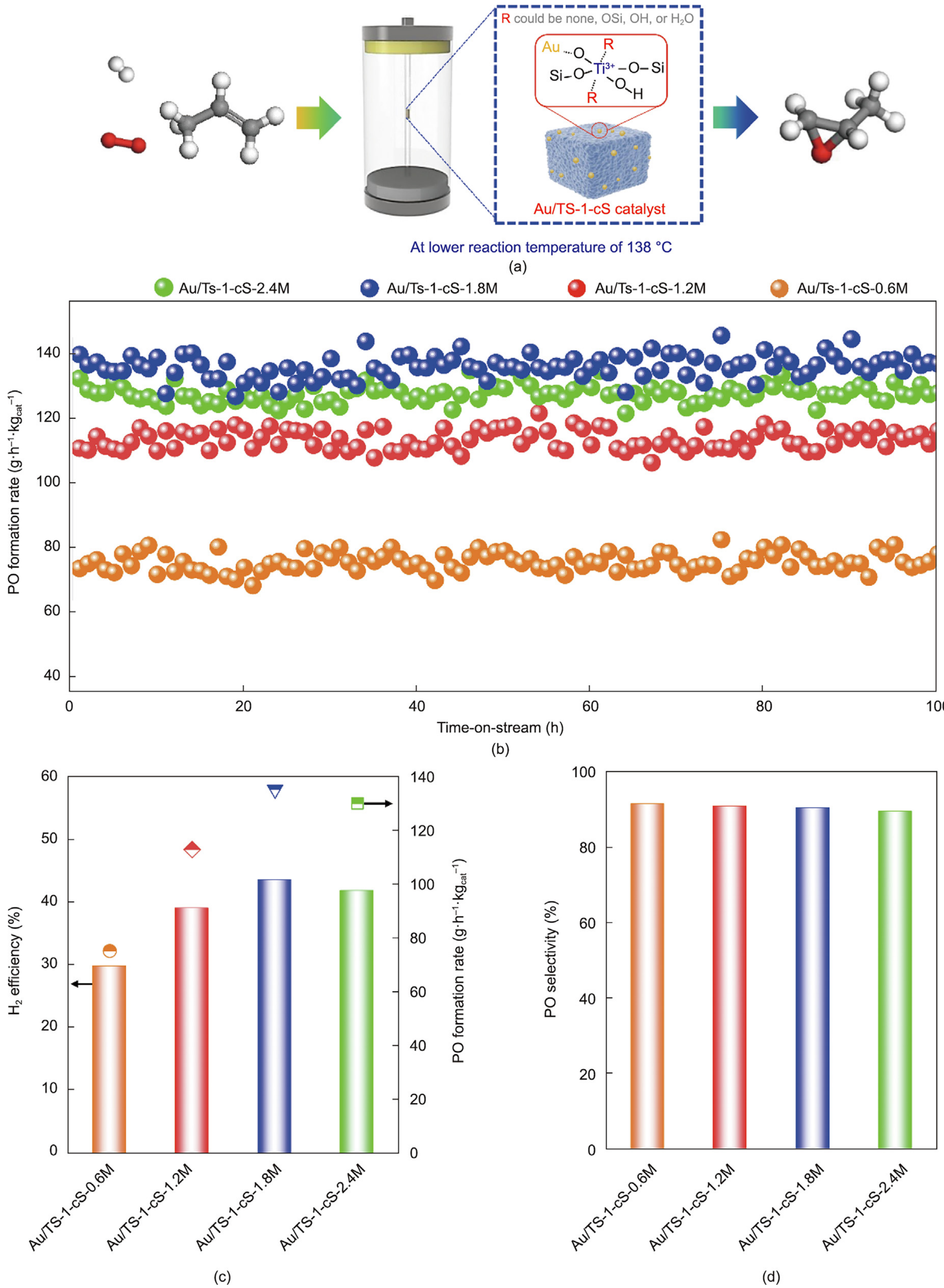

Fig. 2. (a) Reaction process diagram. (b) PO formation rate, (c) H_2 efficiency, and (d) PO selectivity of the Au/TS-1-cS-0.6M, Au/TS-1-cS-1.2M, Au/TS-1-cS-1.8M, and Au/TS-1-cS-2.4M catalysts at the low reaction temperature of 138 °C. kg_{cat}: kilogram of catalyst.

similar synthesis conditions. These results can eliminate the influences of zeolite crystal morphology and size on the catalytic performance. Figs. 4(j) and (k) display the XRD spectra of the three TS-1-cS supports. It is clear that all the TS-1-cS supports exhibit characteristic peaks at 7.8°, 8.8°, 23.1°, 23.9°, and 24.3°, which agree well with the peaks of a typical MFI topological structure.

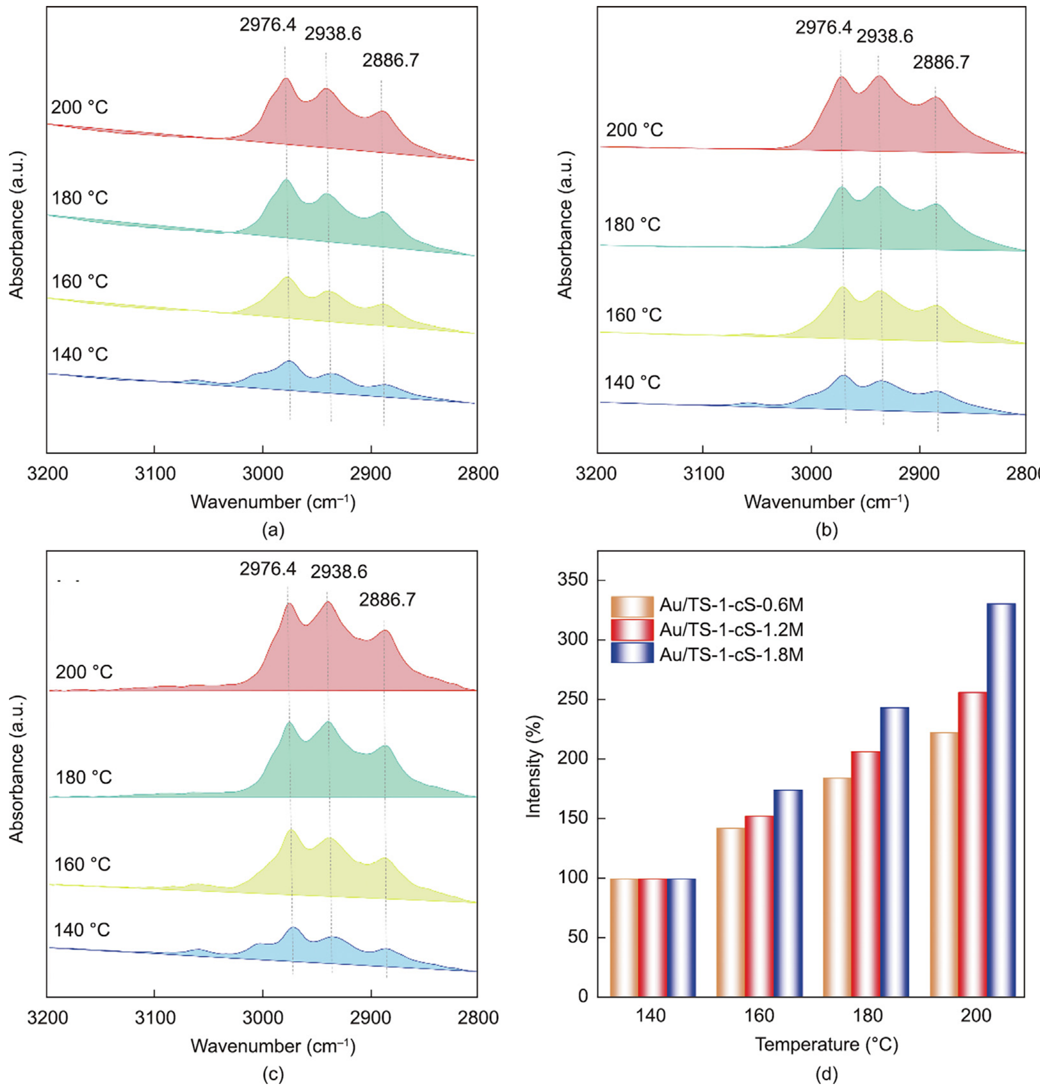

Fig. 3. *In situ* FT-IR spectroscopy results of the (a) Au/TS-1-cS-0.6M, (b) Au/TS-1-cS-1.2M, and (c) Au/TS-1-cS-1.8M catalysts under propene epoxidation conditions (the relative flow rate of C_3H_6, H_2, O_2, and N_2 is 1:1:1:7). (d) *In situ* FT-IR peak intensity of the bidentate propoxy species of the three Au/TS-1-cS catalysts at different reaction temperatures.

In addition, the single diffraction peak at $2\theta = 24.3°$ for all three TS-1-cS supports indicates a structure with orthorhombic symmetry and the incorporation of Ti in the framework [66].

The N_2 physisorption results for Au/TS-1-cS-0.6M, Au/TS-1-cS-1.2M, and Au/TS-1-cS-1.8M are shown in Fig. 4(l) and Table S2 in Appendix A. It can be seen that the N_2 adsorption–desorption isotherms of the three samples are all type-IV isotherms, according to the International Union of Pure and Applied Chemistry (IUPAC)'s classification, which is typical of mesostructured materials. Moreover, with a change in the S-1-*x*M seed, the surface area and total pore volume of the three samples do not change significantly, which can exclude the influence of pore structure on the catalytic performance. In conclusion, after excluding the size effect of Au nanoparticles and of the structure and crystal morphology of the supports, it is speculated that the key factors affecting the catalytic performance involve the titanium species and the metal–support interaction. Therefore, the relationship between the content of the coordinatively unsaturated Ti^{3+} sites and H_2 efficiency was investigated; Fig. 4(n) shows the results, which exhibit an obvious linear relationship.

It is supposed that there are two kinds of Ti species around Au sites in Au/Ti-based catalysts: One kind is adjacent to isolated Ti^{4+} species [6], and the other is adjacent to coordinatively unsaturated Ti^{3+} species. It is widely recognized that H_2O_2 formed around traditional Au–O–Ti^{4+} sites can migrate to the surrounding Ti^{4+} sites to form the Ti–OOH intermediate. However, based on the catalytic performance and structural parameters of the series of Au/TS-1-cS catalysts, we consider that the formation rate of the Ti–OOH intermediate is higher on coordinatively unsaturated Au–O–Ti^{3+} sites than on traditional Au–O–Ti^{4+} sites. We resorted to *operando* UV–vis, XPS, and DFT to explore the structure–performance relationship between different Au–O–Ti sites and H_2 efficiency. *Operando* UV–vis spectroscopy was employed to analyze the change in the Ti–OOH intermediates of the Au/TS-1-cS-0.6M, Au/TS-1-cS-1.2M, and Au/TS-1-cS-1.8M catalysts with different contents of coordinatively unsaturated Ti^{3+} under real reaction conditions. Fig. 5 displays the different peak intensities of the Ti–OOH intermediate, which shows up at approximately 360 nm [67] at various reaction temperatures. In the temperature range of 60–140 °C, the Ti–OOH formation rates of all the Au/TS-1-cS catalysts increase with a rise in reaction temperature. The Au/TS-1-cS-1.8M catalyst with the highest content of coordinatively unsaturated Ti^{3+} sites exhibits the highest Ti–OOH intermediate formation rate in the temperature range of 60–140 °C, which is necessarily

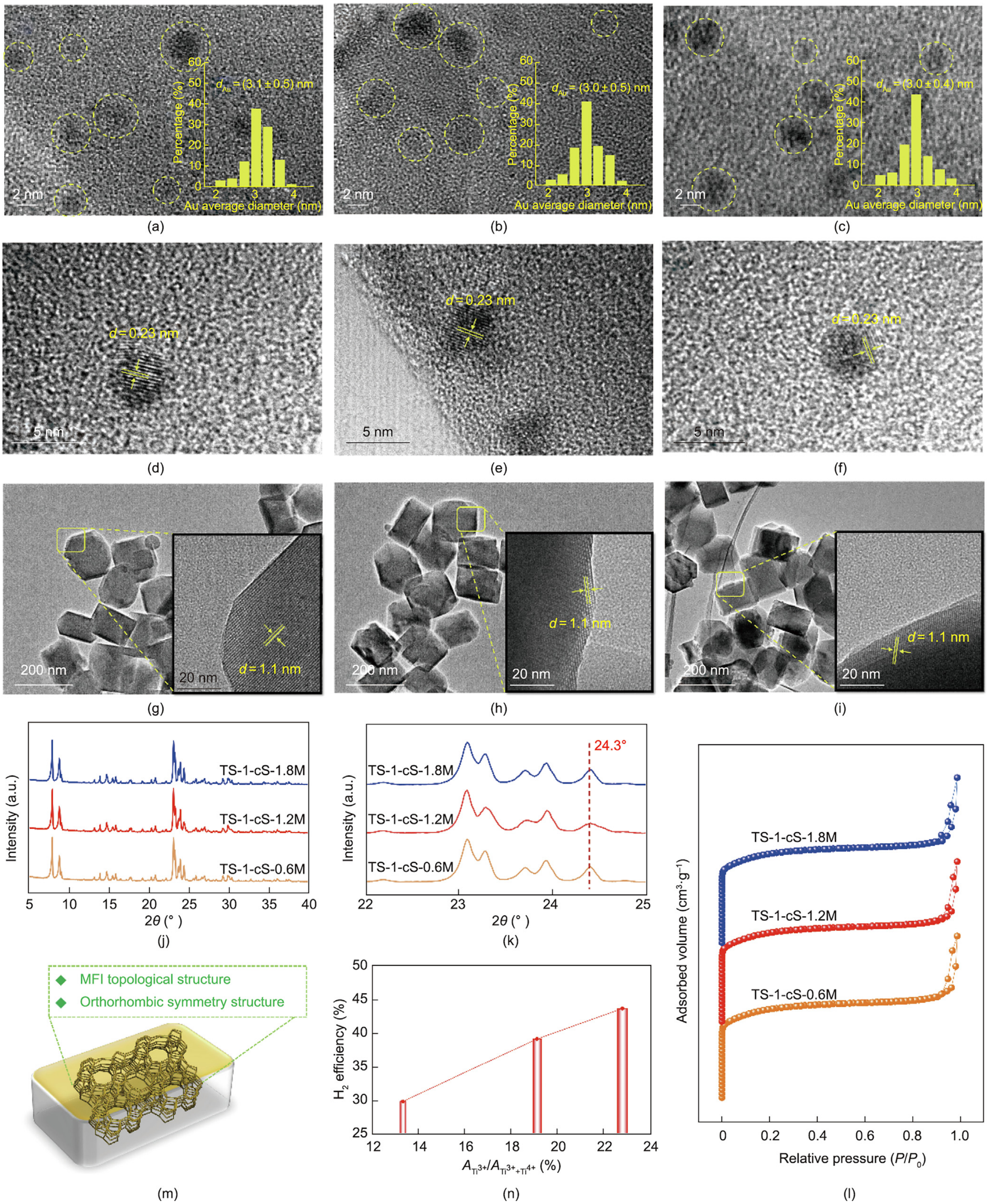

Fig. 4. HRTEM images and Au size distributions for the (a, d) Au/TS-1-cS-0.6M, (b, e) Au/TS-1-cS-1.2M, and (c, f) Au/TS-1-cS-1.8M catalysts. (g–i) TEM images of the (g) Au/TS-1-cS-0.6M, (h) Au/TS-1-cS-1.2M, and (i) Au/TS-1-cS-1.8M catalysts. (j, k) XRD patterns of the TS-1-cS supports. (l) N_2 adsorption–desorption isotherms of the TS-1-cS supports. (m) Crystal structure diagram of the TS-1-cS supports. (n) Relationship between the content of coordinatively unsaturated Ti^{3+} sites and H_2 efficiency.

related to the highest H_2 efficiency and PO formation rate of the Au/TS-1-cS-1.8M catalyst at 138 °C. It is speculated that the outstanding Ti–OOH formation rate derives from the Au–O–Ti^{3+} bifunctional active sites, which can effectively improve the generation of H_2O_2 and the further formation of the active Ti–OOH intermediate. The form of the Au–O–Ti^{3+} bifunctional active sites is

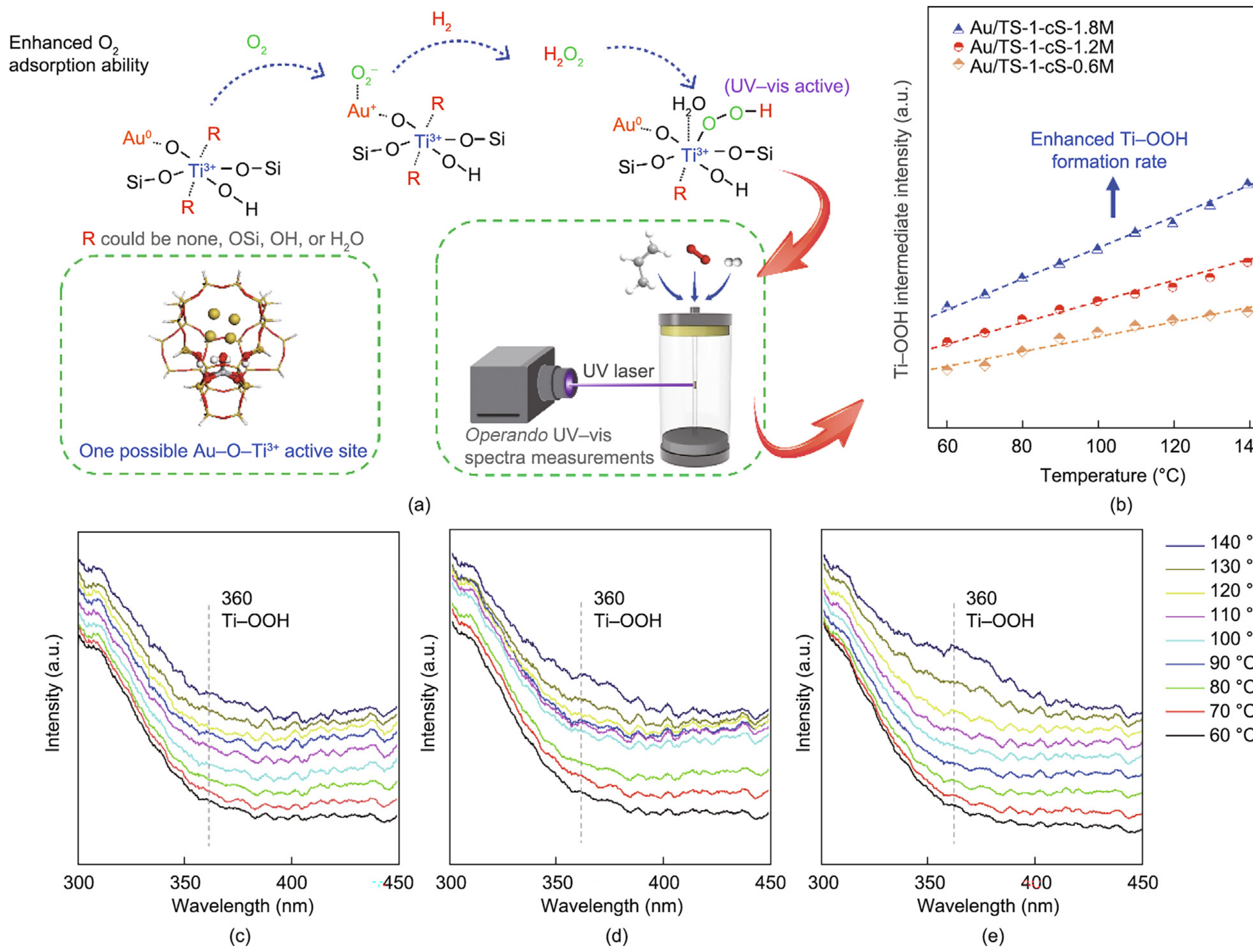

Fig. 5. (a) Diagram of the possible reaction path. (b) Ti–OOH intermediate intensity versus temperature of the Au/TS-1-cS-0.6M, Au/TS-1-cS-1.2M, and Au/TS-1-cS-1.8M catalysts via *operando* UV–vis. (c–e) *Operando* UV–vis spectra of (c) Au/TS-1-cS-0.6M, (d) Au/TS-1-cS-1.2M, and (e) Au/TS-1-cS-1.8M catalysts at different reaction temperatures.

provided in Fig. 5(a), where R is mainly used to show all the possible types of Ti^{3+} species. Based on the catalytic performance of the different Au/TS-1-cS catalysts, the use of different S-1 seeds may only change the number of a dominant R group and not the type of R group.

In order to confirm that coordinatively unsaturated Ti^{3+} sites can anchor the Au precursor to form Au–O–Ti^{3+} bifunctional active sites, XPS was employed to demonstrate the interaction between Au and Ti. Fig. 6 shows the XPS spectra for the Ti 2p and Au 4f of fresh Au/TS-1-cS-0.6M, Au/TS-1-cS-1.2M, and Au/TS-1-cS-1.8M catalysts. The detailed fitting analysis in Figs. 6(a)–(c) show that, for each Ti valence state, there are two peaks separated by about 5.7 eV, corresponding to the $2p_{1/2}$ (higher BE) and $2p_{3/2}$ (lower BE) spin orbit states. Based on previous studies, the high-BE component of Ti $2p_{3/2}$ at 460.03 eV and of Ti $2p_{1/2}$ at 465.73 eV are assigned to framework tetracoordinated Ti^{4+} species, while the low-BE component of Ti $2p_{3/2}$ at 458.02 eV and of Ti $2p_{1/2}$ at 463.72 eV are assigned to framework and/or extra-framework Ti^{3+} species [25,51,68]. It was found that the content of the Ti^{3+} species exhibited a regular increasing trend from fresh Au/TS-1-cS-0.6M to fresh Au/TS-1-cS-1.8M, which is consistent with the UV–vis, ^{31}P MAS NMR, and NH_3-TPD characterization results given in Section 3.1. Moreover, with an increase in the Ti^{3+} content in the catalysts, the BEs of the Ti $2p_{3/2}$ and Ti $2p_{1/2}$ peaks in the catalysts slightly downshift, demonstrating that the charge of the Ti ions in the catalysts becomes more negative with an increase in Ti^{3+} content.

The specific fitting analysis indicated that, for each Au valence state, there are two peaks separated by about 3.7 eV, corresponding to $4f_{5/2}$ (higher BE) and $4f_{7/2}$ (lower BE) spin orbit states (with an intensity ratio of 3/4). According to the literature, the low-BE-component peaks (for Au $4f_{7/2}$) at 83.55, 84.72, and 86.11 eV are assigned to the Au^0, Au^+, and Au^{3+} species, respectively, while the high-BE-component peaks (for Au $4f_{5/2}$) at 87.25, 88.42, and 89.81 eV are assigned to the Au^0, Au^+ and Au^{3+} species, respectively [69–71]. As shown in Figs. 6(d)–(f), with an increase in the Ti^{3+} content in the catalysts, the binding energies of the peaks for the Au 4f in the catalysts upshift slightly. As this is combined with a downshift in the Ti 2p BE, it can be speculated that electrons have been transferred between Au and Ti, indicating that the introduction of coordinatively unsaturated Ti^{3+} sites enhances the immobilization of Au clusters on the TS-1-cS support. This enhancement could be conducive to activating O_2 and H_2 to generate more hydroperoxide active intermediate, which probably promotes the catalytic performance. Furthermore, the content of the Au^+ and Au^{3+} species exhibits a regular increasing trend with an increase in the coordinatively unsaturated Ti^{3+} content in the catalysts. This could be because the coordinatively unsaturated Ti^{3+} sites are more likely to anchor the Au complexes ($[AuCl_x(OH)_{4-x}]^-$) [72]. However, the initial valence state of the Au species has little effect on the catalytic performance, because the catalyst is reduced before the reaction.

In order to further investigate the effect of Ti species with different coordination forms on Au metal and the effect of Au/Ti bifunctional sites with different forms on the direct gas-phase

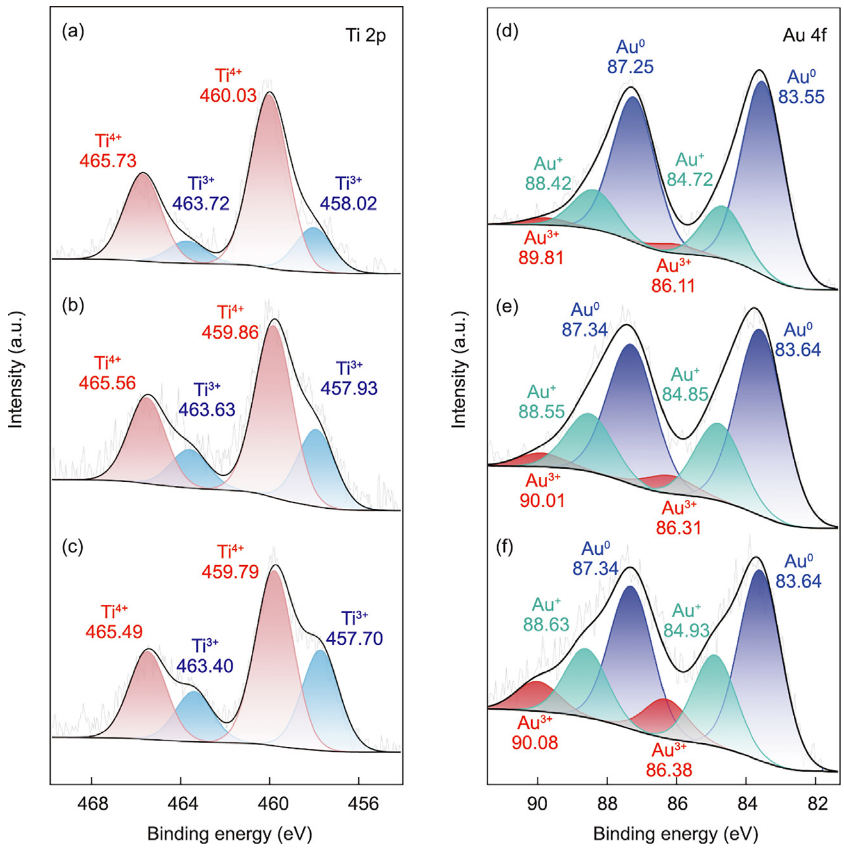

Fig. 6. (a–c) Ti 2p and (d–f) Au 4f XPS spectra, respectively, of fresh (a, d) Au/TS-1-cS-0.6M, (b, e) Au/TS-1-cS-1.2M, and (c, f) Au/TS-1-cS-1.8M catalysts.

propene epoxidation reaction, a DFT study was performed. According to the above characterization results, TS-1-Ti^{4+} and TS-1-Ti^{3+} were constructed to represent perfect tetracoordinated Ti species (Ti^{4+}) and coordinatively unsaturated hexacoordinated Ti species (Ti^{3+}) structures, respectively (Figs. 7(a) and (b)). The Au_4 clusters were further supported on TS-1-Ti^{4+} and TS-1-Ti^{3+} to obtain Au_4/TS-1-Ti^{4+} and Au_4/TS-1-Ti^{3+} models (corresponding to the Au/TS-1-cS-0.6M and Au/TS-1-cS-1.8M catalysts). Fig. 7(c) shows that the Au_4/TS-1-Ti^{3+} model (−153.1 kcal·mol^{-1}, 1 kcal = 4185.85 J) exhibits a much higher BE of the Au_4 cluster than the Au_4/TS-1-Ti^{4+} model (−44.0 kcal·mol^{-1}), indicating that the introduction of coordinatively unsaturated Ti^{3+} sites enhances the immobilization of Au clusters on the TS-1 support. Moreover, Table 1 shows that the Au atoms in the Au_4/TS-1-Ti^{3+} model have stronger electropositivity than those in the Au_4/TS-1-Ti^{4+} model, which is consistent with the XPS result. This finding suggests that the coordinatively unsaturated Ti^{3+} sites promote electron transfer from the Au to Ti species, leading to stronger interaction between the Au clusters and the support.

Subsequently, the adsorption of O_2 over the two models was investigated to reveal the O_2 adsorption ability. Fig. 7(d) clearly shows that a higher O_2 adsorption energy is obtained with the Au_4/TS-1-Ti^{3+} model (−18.1 kcal·mol^{-1}). Furthermore, the positive charge of the O atom in the Au_4/TS-1-Ti^{3+} model is significantly higher than that in the Au_4/TS-1-Ti^{4+} model. This result suggests that the back-donating interaction between Au and O_2 is greatly enhanced due to the presence of coordinatively unsaturated Ti^{3+} sites. It has been demonstrated that enhancing the O_2 adsorption ability promotes the formation of O_2^-, which plays a critical role in boosting the catalytic performance in propene epoxidation. In essence, the formation of coordinatively unsaturated Ti^{3+} sites enhances the interaction between Au and the support and induces the formation of partial positively charged Au species. As a result, the adsorption of O_2 is significantly improved, granting the Au/TS-1-cS-1.8M catalysts an excellent low-temperature catalytic performance. To further confirm the results from DFT, O_2 TPD characterization was performed, as shown in Fig. S6 in Appendix A. The oxygen species can generally be identified as surface oxygen species (< 350 °C), active lattice oxygen species near the surface (350–550 °C), and lattice oxygen species (> 550 °C). As shown in Fig. S6, the desorption capacity of O_2 gradually increases as the number of coordinatively unsaturated Ti^{3+} sites gradually increases, indicating that the increase in Au–O–Ti^{3+} content is indeed conducive to the adsorption of O_2.

In summary, coordinatively unsaturated Ti^{3+} sites are conducive to anchoring Au ions and forming Au–O–Ti^{3+} bifunctional active sites. These new sites enhance the generation of H_2O_2 (i.e., the key step in the reaction) by boosting the O_2 adsorption ability, which is the main reason for the resulting high H_2 efficiency. With an increase in H_2O_2 concentration, the active Ti–OOH intermediate formation rate is increased, which effectively enhances the low-temperature propene epoxidation performance. The insights revealed here shed new light on the design of high-efficiency catalysts for direct low-temperature propene epoxidation.

4. Conclusions

In this work, we formulated a novel strategy to quantitively construct coordinatively unsaturated Ti^{3+} sites on a novel Au/Ti-based catalyst for propene epoxidation with H_2 and O_2 with a Ti^{3+}/(Ti^{3+} + Ti^{4+}) proportion ranging from 13.3% to 22.8% by tuning the amount of Si–OH and Bu_3NH^+ in post-treated S-1 seeds. Based on *operando* UV–vis, XPS, and DFT calculations, it was found that the presence of coordinatively unsaturated Ti^{3+} sites promoted electron transfer between Au and Ti, thereby facilitating the

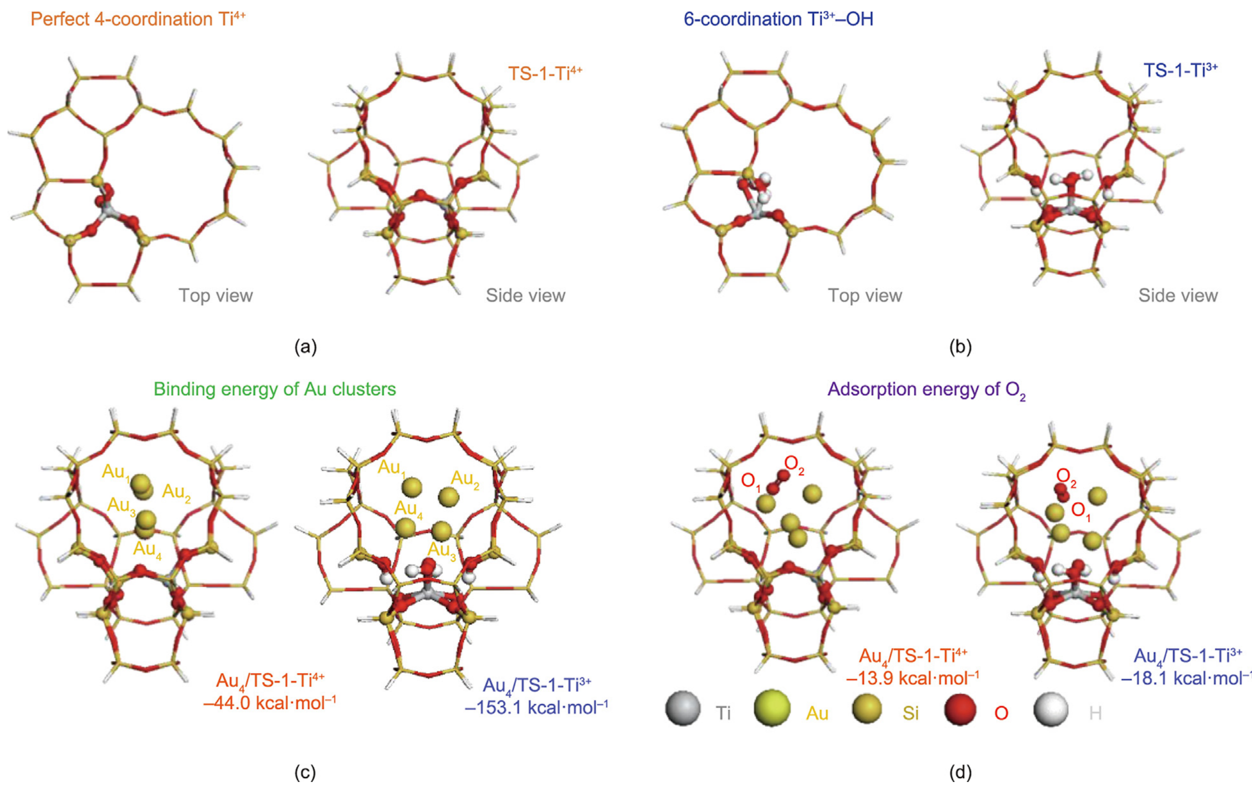

Fig. 7. DFT calculation models of (a) TS-1-Ti^{4+} (perfect 4-coordination Ti) and (b) TS-1-Ti^{3+} (6-coordination Ti^{3+}–OH). (c) Binding energy of Au clusters and (d) adsorption energy of O_2 over Au_4/TS-1-Ti^{4+} and Au_4/TS-1-Ti^{3+} models.

Table 1
Mulliken charge (|*e*|) distribution before and after O_2 adsorption over Au_4/TS-1-Ti^{4+} and Au_4/TS-1-Ti^{3+} models.

Atoms	Before O_2 adsorption		After O_2 adsorption	
	Au_4/TS-1-Ti^{4+}	Au_4/TS-1-Ti^{3+}	Au_4/TS-1-Ti^{4+}	Au_4/TS-1-Ti^{3+}
Au_1	−0.172	−0.142	0.237	0.546
Au_2	0.152	0.057	0.274	0.522
Au_3	0.197	0.289	0.492	0.691
Au_4	−0.081	0.014	0.046	0.612
O_1	–	–	−0.475	−0.525
O_2	–	–	−0.453	−0.522

formation of Au–O–Ti^{3+} active sites. Compared with traditional Au–O–Ti^{4+} sites, these Au–O–Ti^{3+} active sites were found to be more conducive to O_2 adsorption; thus, they effectively promote the *in situ* generation of H_2O_2 and the formation of the active intermediate Ti–OOH. This enables the Au/TS-1-cS catalyst to exhibit excellent hydrogen efficiency (43.6%) and stability than that of traditional Au/Ti-based catalysts at a lower reaction temperature. The insights and strategies reported here open up new opportunities for optimizing H_2 efficiency via a coordinatively unsaturated Ti^{3+} structure on TS-1 and reveal the intrinsic structure–performance relationship of Au/Ti bifunctional catalysts for low-temperature propene epoxidation.

Acknowledgments

This work was supported by the National Natural Science Foundation of China (21978325 and 22122807), Outstanding Youth Fund of the National Natural Science Foundation of China (22122807), Outstanding Youth Fund of Shandong Provincial Natural Science Foundation (ZR2020YQ17), and Natural Science Foundation of Shandong Province (ZR2020KB006).

Compliance with ethics guidelines

Zhaoning Song, Hao Yan, Juncong Yuan, Hongfei Ma, Jianlin Cao, Yongxiang Wang, Qiang Wang, Chong Peng, Feng Deng, Xiang Feng, De Chen, Chaohe Yang, and Yongkang Hu declare that they have no conflict of interest or financial conflicts to disclose.

Appendix A. Supplementary data

Supplementary data to this article can be found online at https://doi.org/10.1016/j.eng.2023.01.008.

References

[1] Lee WS, Cem Akatay M, Stach EA, Ribeiro FH, Delgass WN. Reproducible preparation of Au/TS-1 with high reaction rate for gas phase epoxidation of propylene. J Catal 2012;287:178–89.
[2] Feng X, Duan X, Qian G, Zhou X, Chen D, Yuan W. Insights into size-dependent activity and active sites of Au nanoparticles supported on TS-1 for propene epoxidation with H_2 and O_2. J Catal 2014;317:99–104.
[3] Haruta M, Uphade BS, Tsubota S, Miyamoto A. Selective oxidation of propylene over gold deposited on titanium-based oxides. Res Chem Intermed 1998;24(3):329–36.

[4] Lee WS, Lai LC, Cem Akatay M, Stach EA, Ribeiro FH, Delgass WN. Probing the gold active sites in Au/TS-1 for gas-phase epoxidation of propylene in the presence of hydrogen and oxygen. J Catal 2012;296:31–42.
[5] Chen J, Halin SJA, Pidko EA, Verhoeven MWGMT, Perez Ferrandez DM, Hensen EJM, et al. Enhancement of catalyst performance in the direct propene epoxidation: a study into gold–titanium synergy. ChemCatChem 2013;5 (2):467–78.
[6] Kanungo S, Perez Ferrandez DM, Neira d'Angelo F, Schouten JC, Nijhuis TA. Kinetic study of propene oxide and water formation in hydro-epoxidation of propene on Au/Ti–SiO_2 catalyst. J Catal 2016;338:284–94.
[7] Lu J, Zhang X, Bravo-Suárez JJ, Bando KK, Fujitani T, Oyama ST. Direct propylene epoxidation over barium-promoted Au/Ti–TUD catalysts with H_2 and O_2: effect of Au particle size. J Catal 2007;250(2):350–9.
[8] Song H, Li G, Wang X, Chen Y. Characterization and catalytic performance of Au/Ti–HMS for direct generation of H_2O_2 and *in situ*-H_2O_2-ODS from H_2 and O_2: an *in situ*-reduction synthesis and a recycle study of catalyst. Microporous Mesoporous Mater 2011;139(1–3):104–9.
[9] Yang H, Tang D, Lu X, Yuan Y. Superior performance of gold supported on titanium-containing hexagonal mesoporous molecular sieves for gas-phase epoxidation of propylene with use of H_2 and O_2. J Phys Chem C 2009;113 (19):8186–93.
[10] Nijhuis TA, Sacaliuc-Parvulescu E, Govender NS, Schouten JC, Weckhuysen BM. The role of support oxygen in the epoxidation of propene over gold–titania catalysts investigated by isotopic transient kinetics. J Catal 2009;265 (2):161–9.
[11] Kanungo S, Keshri KS, van Hoof AJF, Neira d'Angelo MF, Schouten JC, Nijhuis TA, et al. Silylation enhances the performance of Au/Ti–SiO_2 catalysts in direct epoxidation of propene using H_2 and O_2. J Catal 2016;344:434–44.
[12] Hayashi T, Tanaka K, Haruta M. Selective vapor-phase epoxidation of propylene over Au/TiO_2 catalysts in the presence of oxygen and hydrogen. J Catal 1998;178(2):566–75.
[13] Song Z, Feng X, Liu Y, Yang C, Zhou X. Advances in manipulation of catalyst structure and relationship of structure–performance for direct propene epoxidation with H_2 and O_2. Prog Chem 2016;28(12):1762–73. Chinese.
[14] Yao S, Xu L, Wang J, Jing X, Odoom-Wubah T, Sun D, et al. Activity and stability of titanosilicate supported Au catalyst for propylene epoxidation with H_2 and O_2. Mol Catal 2018;448:144–52.
[15] Feng X, Sheng N, Liu Y, Chen X, Chen D, Yang C, et al. Simultaneously enhanced stability and selectivity for propene epoxidation with H_2 and O_2 on Au catalysts supported on nano-crystalline mesoporous TS-1. ACS Catal 2017;7 (4):2668–75.
[16] Feng X, Duan X, Qian G, Zhou X, Chen D, Yuan W. Au nanoparticles deposited on the external surfaces of TS-1: enhanced stability and activity for direct propylene epoxidation with H_2 and O_2. Appl Catal B 2014;150–151:396–401.
[17] Bravo-Suárez JJ, Bando KK, Lu J, Haruta M, Fujitani T, Oyama T. Transient technique for identification of true reaction intermediates: hydroperoxide species in propylene epoxidation on gold/titanosilicate catalysts by X-ray absorption fine structure spectroscopy. J Phys Chem C 2008;112(4):1115–23.
[18] Feng X, Yang J, Duan X, Cao Y, Chen B, Chen W, et al. Enhanced catalytic performance for propene epoxidation with H_2 and O_2 over bimetallic Au–Ag/uncalcined TS-1 catalysts. ACS Catal 2018;8(9):7799–808.
[19] Huang J, Takei T, Akita T, Ohashi H, Haruta M. Gold clusters supported on alkaline treated TS-1 for highly efficient propene epoxidation with O_2 and H_2. Appl Catal B 2010;95(3–4):430–8.
[20] Uphade BS, Yamada Y, Akita T, Nakamura T, Haruta M. Synthesis and characterization of Ti–MCM-41 and vapor-phase epoxidation of propylene using H_2 and O_2 over Au/Ti–MCM-41. Appl Catal A 2001;215(1–2):137–48.
[21] Clerici MG. The activity of titanium silicalite-1 (TS-1): some considerations on its origin. Kinet Catal 2015;56(4):450–5.
[22] Xu L, Huang DD, Li CG, Ji X, Jin S, Feng Z, et al. Construction of unique six-coordinated titanium species with an organic amine ligand in titanosilicate and their unprecedented high efficiency for alkene epoxidation. Chem Commun 2015;51(43):9010–903.
[23] Wu L, Deng X, Zhao S, Yin H, Zhuo Z, Fang X, et al. Synthesis of a highly active oxidation catalyst with improved distribution of titanium coordination states. Chem Commun 2016;52(56):8679–82.
[24] Wu L, Tang Z, Yu Y, Yao X, Liu W, Li L, et al. Facile synthesis of a high-performance titanosilicate catalyst with controllable defective $Ti(OSi)_3OH$ sites. Chem Commun 2018;54(49):6384–7.
[25] Zhang Z, Zhao X, Wang G, Xu J, Lu M, Tang Y, et al. Uncalcined TS-2 immobilized Au nanoparticles as a bifunctional catalyst to boost direct propylene epoxidation with H_2 and O_2. AIChE J 2020;66(2):e16815.
[26] Gordon CP, Engler H, Tragl AS, Plodinec M, Lunkenbein T, Berkessel A, et al. Efficient epoxidation over dinuclear sites in titanium silicalite-1. Nature 2020;586(7831):708–13.
[27] Signorile M, Braglia L, Crocellà V, Torelli P, Groppo E, Ricchiardi G, et al. Titanium defective sites in TS-1: structural insights by combining spectroscopy and simulation. Angew Chem Int Ed Engl 2020;59(41):18145–50.
[28] Cundy CS, Forrest JO, Plaisted RJ. Some observations on the preparation and properties of colloidal silicalites. Part I: synthesis of colloidal silicalite-1 and titanosilicalite-1 (TS-1). Microporous Mesoporous Mater 2003;66(2–3):143–56.
[29] Khomane RB, Kulkarni BD, Paraskar A, Sainkar SR. Synthesis, characterization and catalytic performance of titanium silicalite-1 prepared in micellar media. Mater Chem Phys 2002;76:99–103.
[30] Lee WS, Cem Akatay M, Stach EA, Ribeiro FH, Delgass WN. Enhanced reaction rate for gas-phase epoxidation of propylene using H_2 and O_2 by Cs promotion of Au/TS-1. J Catal 2013;308:98–113.
[31] Zhuang J, Han X, Bao X. *In-situ* ^{31}P MAS NMR probing of the active centers in Ti silicalite molecular sieve. Catal Commun 2015;62:75–8.
[32] Kapil N, Weissenberger T, Cardinale F, Trogadas P, Nijhuis TA, Nigra MM, et al. Precisely engineered supported gold clusters as a stable catalyst for propylene epoxidation. Angew Chem Int Ed Engl 2021;60(33):18185–93.
[33] Wu L, Zhao S, Lin L, Fang X, Liu Y, He M. In-depth understanding of acid catalysis of solvolysis of propene oxide over titanosilicates and titanosilicate/H_2O_2 systems. J Catal 2016;337:248–59.
[34] Zhuang J, Ma D, Yan Z, Deng F, Liu X, Han X, et al. Solid-state MAS NMR detection of the oxidation center in TS-1 zeolite by *in situ* probe reaction. J Catal 2004;221(2):670–3.
[35] Yi X, Liu K, Chen W, Li J, Xu S, Li C, et al. Origin and structural characteristics of tri-coordinated extra-framework aluminum species in dealuminated zeolites. J Am Chem Soc 2018;140(34):10764–74.
[36] Gao P, Wang Q, Xu J, Qi G, Wang C, Zhou X, et al. Brønsted/Lewis acid synergy in methanol-to-aromatics conversion on Ga-modified ZSM-5 zeolites, as studied by solid-state NMR spectroscopy. ACS Catal 2018;8(1):69–74.
[37] Li Z, Wang Y, Zhang J, Wang D, Ma W. Better performance for gas-phase epoxidation of propylene using H_2 and O_2 at lower temperature over Au/TS-1 catalyst. Catal Commun 2017;90:87–90.
[38] Song Z, Yuan J, Cai Z, Lin D, Feng X, Sheng N, et al. Engineering three-layer core–shell S-1/TS-1@dendritic-SiO_2 supported Au catalysts towards improved performance for propene epoxidation with H_2 and O_2. Green Energy Environ 2020;5(4):473–83.
[39] Xu H, Zhang Y, Wu H, Liu Y, Li X, Jiang J, et al. Postsynthesis of mesoporous MOR-type titanosilicate and its unique catalytic properties in liquid-phase oxidations. J Catal 2011;281(2):263–72.
[40] Li D, Xing B, Wang B, Li R. Theoretical study of zirconium isomorphous substitution into zeolite frameworks. Molecules 2019;24(24):4466.
[41] Yue Q, Zhang J, Shamzhy M, Opanasenko M. Seeded growth of isomorphously substituted chabazites in proton-form. Microporous Mesoporous Mater 2019;280:331–6.
[42] Zhang S, Liu X, Zhang Y, Lv T, Zheng J, Gao W, et al. Study on the synthesis of MFI and FER in the presence of *n*-butylamine and the property of *n*-butylamine in a confined region of zeolites. RSC Adv 2016;6(115):114808–17.
[43] Sun Y, Ma T, Cao S, Wang J, Meng X, Gong Y, et al. Defective sites in ZSM-5 zeolite synthesized by *n*-butylamine template facilitating uniform meso-microporosity by alkali-treatment. Microporous Mesoporous Mater 2021;326:111360.
[44] Ione KG, Vostrikova LA, Mastikhin VM. Synthesis of crystalline metal silicates having zeolite structure and study of their catalytic properties. J Mol Catal 1985;31(3):355–70.
[45] Wang X, Guo X, Li G. Synthesis of titanium silicalite (TS-1) from the TPABr system and its catalytic properties for epoxidation of propylene. Catal Today 2002;74(1–2):65–75.
[46] Song Z, Feng X, Sheng N, Lin D, Li Y, Liu Y, et al. Cost-efficient core–shell TS-1/silicalite-1 supported Au catalysts: towards enhanced stability for propene epoxidation with H_2 and O_2. Chem Eng J 2019;377:119927.
[47] Sheng N, Liu Z, Song Z, Lin D, Feng X, Liu Y, et al. Enhanced stability for propene epoxidation with H_2 and O_2 over wormhole-like hierarchical TS-1 supported Au nanocatalyst. Chem Eng J 2019;377:119954.
[48] Mul G, Zwijnenburg A, van der Linden B, Makkee M, Moulijn JA. Stability and selectivity of Au/TiO_2 and Au/TiO_2/SiO_2 catalysts in propene epoxidation: an *in situ* FT-IR study. J Catal 2001;201(1):128–37.
[49] Lu X, Zhao G, Lu Y. Propylene epoxidation with O_2 and H_2: a high-performance Au/TS-1 catalyst prepared via a deposition–precipitation method using urea. Catal Sci Technol 2013;3(11):2906–9.
[50] Guo Q, Sun K, Feng Z, Li G, Guo M, Fan F, et al. A thorough investigation of the active titanium species in TS-1 zeolite by *in situ* UV resonance Raman spectroscopy. Chemistry Eur J 2012;18(43):13854–60.
[51] Xu J, Zhang Z, Wang G, Duan X, Qian G, Zhou X. Zeolite crystal size effects of Au/uncalcined TS-1 bifunctional catalysts on direct propylene epoxidation with H_2 and O_2. Chem Eng Sci 2020;227:115907.
[52] Feng X, Duan X, Cheng H, Qian G, Chen D, Yuan W, et al. Au/TS-1 catalyst prepared by deposition–precipitation method for propene epoxidation with H_2/O_2: insights into the effects of slurry aging time and Si/Ti molar ratio. J Catal 2015;325:128–35.
[53] Whittaker T, Kumar KBS, Peterson C, Pollock MN, Grabow LC, Chandler BD. H_2 oxidation over supported Au nanoparticle catalysts: evidence for heterolytic H_2 activation at the metal–support interface. J Am Chem Soc 2018;140 (48):16469–87.
[54] Lewis RJ, Hutchings GJ. Recent advances in the direct synthesis of H_2O_2. ChemCatChem 2019;11(1):298–308.
[55] Jin Z, Liu Y, Wang L, Wang C, Wu Z, Zhu Q, et al. Direct synthesis of pure aqueous H_2O_2 solution within aluminosilicate zeolite crystals. ACS Catal 2021;11(4):1946–51.
[56] Lee WS, Cem Akatay M, Stach EA, Ribeiro FH, Delgass WN. Gas-phase epoxidation of propylene in the presence of H_2 and O_2 over small gold ensembles in uncalcined TS-1. J Catal 2014;313:104–12.
[57] Qi C, Huang J, Bao S, Su H, Akita T, Haruta M. Switching of reactions between hydrogenation and epoxidation of propene over Au/Ti-based oxides in the presence of H_2 and O_2. J Catal 2011;281(1):12–20.

[58] Feng X, Duan X, Yang J, Qian G, Zhou X, Chen D, et al. Au/uncalcined TS-1 catalysts for direct propene epoxidation with H_2 and O_2: effects of Si/Ti molar ratio and Au loading. Chem Eng J 2015;278:234–9.
[59] Huang J, Lima E, Akita T, Guzmán A, Qi C, Takei T, et al. Propene epoxidation with O_2 and H_2: identification of the most active gold clusters. J Catal 2011;278(1):8–15.
[60] Ishida T, Kinoshita N, Okatsu H, Akita T, Takei T, Haruta M. Influence of the support and the size of gold clusters on catalytic activity for glucose oxidation. Angew Chem Int Ed Engl 2008;47(48):9265–8.
[61] Song Z, Feng X, Sheng N, Lin D, Li Y, Liu Y, et al. Propene epoxidation with H_2 and O_2 on Au/TS-1 catalyst: cost-effective synthesis of small-sized mesoporous TS-1 and its unique performance. Catal Today 2018;347: 102–9.
[62] Feng X, Song Z, Liu Y, Chen X, Jin X, Yan W, et al. Manipulating gold spatial location on titanium silicalite-1 to enhance the catalytic performance for direct propene epoxidation with H_2 and O_2. ACS Catal 2018;8(11):10649–57.
[63] Chen D, Moljord K, Fuglerud T, Holmen A. The effect of crystal size of SAPO-34 on the selectivity and deactivation of the MTO reaction. Microporous Mesoporous Mater 1999;29(1–2):191–203.
[64] Zhang T, Chen X, Chen G, Chen M, Bai R, Jia M, et al. Synthesis of anatase-free nano-sized hierarchical TS-1 zeolites and their excellent catalytic performance in alkene epoxidation. J Mater Chem A 2018;6(20):9473–9.
[65] Yuan J, Song Z, Lin D, Feng X, Tuo Y, Zhou X, et al. Mesoporogen-free strategy to construct hierarchical TS-1 in a highly concentrated system for gas-phase propene epoxidation with H_2 and O_2. ACS Appl Mater Interfaces 2021;13 (22):26134–42.
[66] Feng X, Liu Y, Li Y, Yang C, Zhang Z, Duan X, et al. Au/TS-1 catalyst for propene epoxidation with H_2/O_2: a novel strategy to enhance stability by tuning charging sequence. AIChE J 2016;62(11):3963–72.
[67] Zhang M, Zhang S, Meng F, Hu M, Wang Z, Zeng Y, et al. Catalytic peroxone process for low-temperature denitration with enhanced Ti–OOH formation on P-TiO_2: experimental, DFT, and semi-*in-situ* UV–vis studies. Fuel 2022;330:125664.
[68] Kim SK, Reddy BM, Park SE. High-performance microwave synthesized mesoporous TS-1 zeolite for catalytic oxidation of cyclic olefins. Ind Eng Chem Res 2018;57(10):3567–74.
[69] Lin D, Zhang Q, Qin Z, Li Q, Feng X, Song Z, et al. Reversing titanium oligomer formation towards high-efficiency and green synthesis of titanium-containing molecular sieves. Angew Chem Int Ed Engl 2021;60(7):3443–8.
[70] Lin D, Zheng X, Feng X, Sheng N, Song Z, Liu Y, et al. Enhancing the dynamic electron transfer of Au species on wormhole-like TS-1 for boosting propene epoxidation performance with H_2 and O_2. Green Energy Environ 2020;5 (4):433–43.
[71] Zhou K, Wang W, Zhao Z, Luo G, Miller JT, Wong MS, et al. Synergistic gold–bismuth catalysis for non-mercury hydrochlorination of acetylene to vinyl chloride monomer. ACS Catal 2014;4(9):3112–6.
[72] Zanella R, Delannoy L, Louis C. Mechanism of deposition of gold precursors onto TiO_2 during the preparation by cation adsorption and deposition–precipitation with NaOH and urea. Appl Catal A 2005;291(1–2):62–72.